

1 **A Study of Earthquake Recurrence based on a One-body**
2 **Spring-slider Model in the Presence of Thermal-pressurized**
3 **Slip-weakening Friction and Viscosity**

4
5 Jeen-Hwa Wang

6 Institute of Earth Sciences, Academia Sinica, P.O. Box 1-55, Nangang, Taipei,
7 TAIWAN (e-mail: jhwang@earth.sinica.edu.tw)

8 (submitted to Natural Hazards and Earth System Sciences on December 29, 2017;
9 re-submitted on January 18, 2018; revised on June 4, 2018)

10

11 **Abstract** Earthquake recurrence is studied from the temporal variation in slip
12 through numerical simulations based on the normalized form of equation of motion of
13 a one-body spring-slider model with thermal-pressurized slip-weakening friction and
14 viscosity. The wear process, whose effect is included in the friction law, is also taken
15 into account in this study. The main parameters are the normalized characteristic
16 displacement, U_c , of the friction law and the normalized damping coefficient (to
17 represent viscosity), η . Define T_R , D , and τ_D to be the recurrence time of events, the
18 final slip of an event, and the duration time of an event, respectively. Simulation
19 results show that T_R increases when U_c decreases or η increases; D and τ_D decrease
20 with increasing η ; and τ_D increases with U_c . The time- and slip-predictable model can
21 describe the temporal variation in cumulative slip. When the wear process is
22 considered, the thickness of slip zone, h which depends on the cumulated slip,
23 $S(t)=\sum D(t)$, i.e., $h(t)=CS(t)$ (C =a dimensionless increasing rate of h with S) is an
24 important parameter influencing T_R and D . U_c is a function of h and thus depends on

25 cumulated slip, $\sum U$, with an increasing rate of C . In the computational time period,
26 the wear process influences the recurrence of events and such an effect increases with
27 C when $C > 0.0001$. When viscosity is present, the effect due to wear process becomes
28 stronger. Both T_R and D decrease when the fault becomes more mature, thus
29 suggesting that it is more difficult to produce large earthquakes along a fault when it
30 becomes more mature. Neither the time-predictable model nor the slip-predictable one
31 can describe the temporal variation in cumulative slip of earthquakes under the wear
32 process with large C .

33

34 **Key Words:** Recurrence of earthquakes, final slip, rise time, one-body spring-slider
35 model, thermal-pressurized slip-weakening friction, characteristic displacement,
36 viscosity, wear process

37

38 **1 Introduction**

39 Earthquake recurrence that is relevant to the physics of faulting is an important
40 factor in seismic hazard assessment. It is related to the seismic cycle, which represents
41 the occurrence of several earthquakes in the same segment of a fault during a time
42 period. Fig. 1 exhibits the general pattern of time variation in slip and particle velocity
43 during a seismic cycle. In the figure, T_R is the recurrence (also denoted by repeat or
44 inter-event) time of two events in a seismic cycle, τ_D is the duration time of slip of an
45 event, D is the final slip of an event, and V_m is the peak value of particle velocity of
46 an event. The four parameters could be constants in the time history when all model
47 parameters do not vary with time and could also vary with time, represented by $T_R(t)$,
48 $\tau_D(t)$, $D(t)$, and $V_m(t)$, when one of model parameters does vary with time. Sykes and
49 Quittmeyer (1981) pointed out that the major factors in controlling T_R are the plate

50 moving speed and the geometry of the rupture zone. Based on Reid's elastic rebound
51 theory (Reid, 1910), Schwartz and Coppersmith (1984) assumed that an earthquake
52 occurs when the tectonic shear stress on a fault is higher than a critical level, which is
53 dependent on the physical conditions of the fault and the loading by regional tectonics.
54 Since in their work a fault has a homogeneous distribution of physical properties
55 under constant tectonic loading, earthquakes could happen regularly.

56 Some observations exhibit periodicity for different size earthquakes. Bakun and
57 McEvilly (1979) obtained $T_R \approx 23 \pm 9$ years for $M \approx 6$ earthquakes at the Parkfield
58 segment of the San Andreas fault, USA since 1857. Sykes and Menke (2006)
59 estimated $T_R \approx 100$ years for $M \geq 8$ earthquakes in the Nankaido segments of the Nankai
60 trough, Japan. Okada et al. (2003) gained $T_R = 5.5 \pm 0.7$ years for earthquakes with
61 $M = 4.8 \pm 0.1$ off Kamaishi, Japan, since 1957. Nadeau and Johnson (1998) inferred an
62 empirical relation between T_R and seismic moment, M_o : $T_R \propto M_o^{1/6}$. To make this
63 relation valid, the stress drop, $\Delta\sigma$, or the long-term slip velocity of a fault, v_l , must be
64 in terms of M_o . Based on three data set from eastern Taiwan, Parkfield, USA, and
65 northeastern Japan, Chen et al. (2007) inferred $T_R \sim M_o^{0.61}$. Beeler et al. (2001)
66 proposed a theoretical relation: $T_R = \Delta\sigma^{2/3} M_o^{1/3} / 1.81 \mu v_l$, where μ is the rigidity of the
67 fault-zone materials.

68 However, the main factors in influencing earthquake occurrences commonly are
69 spatially heterogeneous and also vary with time. Thus, the recurrence times of
70 earthquakes, especially large events, are not constant inferred either from observations
71 (Ando, 1975; Sieh, 1981; Kanamori and Allen, 1986; Wang and Kuo, 1998; Wang,
72 2005; Sieh et al., 2008) or from modeling (Wang, 1995, 1996; Ward, 1996, 2000;
73 Wang and Hwang, 2001). Kanamori and Allen (1986) observed that faults with longer
74 T_R are stronger than those with shorter T_R . Davies et al. (1989) proposed that the

75 longer it has been since the last earthquake, the longer the expected time till the next.
76 Wang and Kuo (1998) observed that for $M \geq 7$ earthquakes in Taiwan T_R strongly
77 follows the Poissonian processes. Enescu et al. (2008) found that the probability
78 density distribution of T_R can be described by an exponential function. From the
79 estimated values of T_R of earthquakes happened on the Chelungpu fault in central
80 Taiwan from trenching data, Wang (2005) found that the earthquakes occurred
81 non-periodically.

82 In order to interpret earthquake recurrences, Shimazaki and Nakata (1980)
83 proposed three simple phenomenological models. Each model has a constantly
84 increasing tectonic stress that is controlled by a critical stress level, σ_c , for failure and
85 a base stress level, σ_b . The three models are: (1) the perfectly periodic model (with
86 constant σ_c , σ_b , and $\Delta\sigma$); (2) the time-predictable model (with constant σ_c , variable
87 σ_b , and variable $\Delta\sigma$); and (3) the slip-predictable model (with variable σ_c , constant σ_b ,
88 and variable $\Delta\sigma$). For the first model, both T_R and D of next earthquake can be
89 predicted from the values of T_R or D of previous ones. For the second model, T_R of
90 next earthquake can be predicted from the values of D of previous ones. For the third
91 model, D of next earthquake can be predicted from the values of T_R of previous ones.
92 However, debates about the three models have been made for a long time. Some
93 examples are given below. Ando (1975) suggested that the second model worked for
94 post-1707 events, yet not for pre-1707 ones in the Nankai trough, Japan. Wang (2005)
95 assumed that the second model could describe the earthquakes occurred on the
96 Chelungpu fault, Taiwan in the past 1900 years. For the Parkfield earthquake
97 sequence, Bakun and McEvilly (1984) took different models; while Murray and
98 Segall (2002) considered the failure of the second model. From laboratory results,
99 Rubinstein et al. (2012) assumed the failure of the time- and slip-predictable models

100 for earthquakes.

101 Some models, for instance the crack model and dynamical spring-slider model,
102 have been developed for fault dynamics, even though the seismologists have not a
103 comprehensive model. There are several factors in controlling fault dynamics and
104 earthquake ruptures (see Bizzarri, 2009; Wang, 2017b). Among the factors, friction
105 (Nur, 1978; Belardinelli and Belardinelli, 1996) and viscosity (Jeffreys, 1942; Spray,
106 1993; Wang, 2007) are two significant ones.

107 Modeling earthquake recurrence based on different models has been long made and
108 is reviewed by Bizzarri (2012a,b) and Franović et al. (2016). Among the models, the
109 spring-slider model has been used to study fault dynamics and earthquake physics
110 (see Wang 2008). Burridge and Knopoff (1967) proposed the one-dimensional
111 N-body model (abbreviated as the 1-D BK model henceforth). Wang (2000, 2012)
112 extended the 1-D model to 2-D one. The one-, two-, three-, and few-body models with
113 various friction laws have also been applied to approach fault dynamics (see Turcotte,
114 1992). The studies for various friction laws based on spring-slider models are briefly
115 described below: (1) for rate- and state-dependent friction (e.g., Rice and Tse, 1986;
116 Ryabov and Ito, 2001; Erickson et al., 2008, 2011; He et al., 2003; Mitsui and
117 Hirahara, 2009; Bizzarri, 2012a; Abe and Kato, 2013; Kostić et al., 2013a; Bizzarri
118 and Crupi, 2014; Franović et al., 2016); (2) for velocity-weakening friction (e.g.,
119 Carlson and Langer, 1989; Huang and Turcotte, 1992; Brun and Gomez, 1994; Wang
120 and Hwang, 2001; Wang, 2003; Kostić et al., 2013b); (3) for simple static/dynamic
121 friction (e.g., Abaimov et al., 2007; Hasumi, 2007).

122 Some results concerning earthquake recurrence are simply explained below.
123 Erickson et al. (2008) suggested that aperiodicity in earthquake dynamics is due to
124 either the nonlinear friction law (Huang and Turcotte, 1990) or the heterogeneous

125 stress distribution (Lapusta and Rice, 2003). Wang and Hwang (2001) emphasized the
126 importance of heterogeneous frictional strengths. Mitsui and Hirahara (2009) pointed
127 out the effect of thermal pressurization. Dragoni and Piombo (2011) found that
128 variable strain rate causes aperiodicity of earthquakes. Bizzarri and Crupi (2014)
129 found that T_R is dependent on the loading rate, effective normal stress, and
130 characteristic distance of the rate- and state-dependent friction law.

131 As mentioned previously, numerous studies have been made for exploring the
132 frictional effect on earthquake recurrence. But, the study concerning the viscous effect
133 on earthquake recurrence is rare. In the followings, we will investigate the effects of
134 slip-weakening friction due to thermal-pressurization and viscosity on earthquake
135 recurrence based on the one-body spring-slider model.

136

137 **2 One-body Model**

138 Fig. 2 displays the one-body spring-slider model. In the model, m , K , N , F , η , u , v
139 ($=du/dt$), v_p , and $u_o=v_p t$ denote, respectively, the mass of the slider, the stiffness (or
140 spring constant) of the leaf spring, the normal force, the frictional force between the
141 slider and the moving plate, the damping coefficient (to represent viscosity as
142 explained below), the displacement of the slider, the velocity of the slider, the plate
143 moving speed, and the equilibrium location of the slider. The frictional force F (with
144 the static value of F_o) is usually a function of u or v . Viscosity results in the viscous
145 force, Φ , between the slider and the moving plate, and Φ is in terms of v . A driving
146 force, $Kv_p t$, caused by the moving plate through the leaf spring pulls the slider to
147 move. The equation of motion of the model is:

148

$$149 \quad md^2u/dt^2 = -K(u-u_o) - F(u,v) - \Phi(v). \quad (1)$$

150

151 When $Kv_p t \geq F_o$, F changes from static frictional force to dynamic one and thus makes
152 the slider move. Among the physical models to approach earthquake faults, the single
153 spring-slider model, which can represent a single fault, is actually the simplest one.
154 However, based on this simple model in the presence of thermal-pressurized friction
155 and viscosity we can obtain good simulations of earthquake recurrences along a single
156 fault. Results can exhibit the frictional and viscous effects on earthquake recurrence.

157 The frictional force $F(u,v)$ is controlled by several factors (see Wang, 2016; and
158 cited references therein). An effect combined from temperature and fluids in a fault
159 zone can result in thermal pressurization (abbreviated as TP below) which would yield
160 a shear stress (resistance) on the fault plane (Sibson, 1973; Lachenbruch, 1980; Rice,
161 2006; Wang, 2009, 2011, 2016, 2017a,b,c; Bizzarri, 2009). Rice (2006) proposed two
162 end-member models of TP, i.e., the adiabatic-undrained-deformation (AUD) model
163 and slip-on-a-plane (SOP) model. Since the characteristic distance of the SOP model
164 cannot be associated with the wear process, the SOP model is not used in this study.
165 The AUD model is related to a homogeneous simple strain ϵ at a constant normal
166 stress σ_n on a spatial scale of the sheared layer. Its shear stress-slip function, $\tau(u)$, is:
167 $\tau(u) = \mu_f(\sigma_n - p_o) \exp(-u/u_c)$ (Rice, 2006), which decreases exponentially with increasing
168 u . The characteristic displacement is $u_c = \rho_f C_v h / \mu_f \Lambda$, where ρ_f , C_v , h , μ_f , and Λ are,
169 respectively, the fluid density, heat capacity (in J/°C/kg), the thickness, frictional
170 strength, and the undrained pressurization factor of the fault zone. The parameter Λ is
171 $(\lambda_f - \lambda_n) / (\beta_f + \beta_n)$ where β_f =isothermal compressibility of the pore fluid, β_n =isothermal
172 compressibility of the pore space, λ_f =isobaric, volumetric thermal expansion
173 coefficient for the pore fluid, and λ_n =isobaric, volumetric thermal expansion
174 coefficient for the pore space.

175 Based on the AUD model, Wang (2009, 2016, 2017a,b,c) took a simplified slip-
176 weakening friction law (denoted by the TP law hereafter):

177

$$178 \quad F(u) = F_o \exp(-u/u_c). \quad (2)$$

179

180 The value of $F(u)$ at $u=0$ is F_o , i.e., the static friction force. An example of the plot of
181 $F(u)$ versus u for five values of u_c , i.e., 0.1, 0.3, 0.5, 0.7, and 0.9 m when $F_o=1 \text{ N/m}^2$,
182 which are taken from Wang (2016), is displayed in Fig. 3. $F(u)$ decreases with
183 increasing u and its decreasing rate, γ , decreases with increasing u_c . The force drop is
184 lower for larger u_c than for smaller u_c for the same final slip. When $u \ll u_c$,
185 $\exp(-u/u_c) \approx 1 - u/u_c$, thus indicating that u_c^{-1} is almost γ at small u . This TP law is used
186 in this study.

187 A detailed description about viscosity and the viscous force $\Phi(\nu)$ can be found in
188 Wang (2016), and only a brief explanation is given below. Jeffreys (1942) first and
189 then numerous authors (Byerlee, 1968; Turcotte and Schubert, 1982; Scholz, 1990;
190 Rice et al., 2001; Wang, 2016) emphasized the viscous effect on faulting due to
191 frictional melts. The viscosity coefficient, ν , of rocks is influenced by T (see Turcotte
192 and Schubert, 1982; Wang, 2011). Spray (2005; and cited references therein) observed
193 a decrease in ν with increasing T . He also stressed that frictional melts with low ν
194 could produce a large volume of melting, thus reducing the effective normal stress.
195 This behaves like fault lubricants during seismic slip.

196 The physical models of viscosity can be found in several articles (e.g., Cohen, 1979;
197 Hudson, 1980). The stress-strain relationship is $\sigma = E\varepsilon$ where σ and E are, respectively,
198 the stress and the elastic modulus for an elastic body and $\sigma = \nu(d\varepsilon/dt)$, where ν is the
199 viscosity coefficient, for a viscous body. Two simple models with a viscous damper

200 and an elastic spring are often used to describe the viscous materials. A viscous
201 damper and an elastic spring are connected in series leading to the Maxwell model
202 and in parallel resulting in the Kelvin-Voigt model (or the Voigt model). According to
203 Hudson (1980), Wang (2016) proposed that the latter is more suitable than the former
204 for seismological problems and thus the Kelvin-Voigt model, whose constitution law
205 is $\sigma(t)=E\varepsilon(t)+\nu d\varepsilon(t)/dt$, is taken here and displayed in Fig. 2. The viscous stress is νv .

206 In order to investigate the viscous effect in a dynamical system, Wang (2016)
207 defined the damping coefficient, η , based on the phenomenon that an oscillating body
208 damps in viscous fluids. According to Stokes' law, $\eta=6\pi R\nu$ for a sphere of radius R in
209 a viscous fluid of ν (see Kittel et al., 1968). Hence, the viscous force in Equation 1 is
210 represented by $\Phi=\eta v$. Note that the unit of η is $\text{N}(\text{m/s})^{-1}$. Since ν decreases with
211 increasing T , η decreases with increasing T . Hence, η can vary with time during
212 faulting. This point has been studied by Wang (2017b) for the generation of nuclear
213 phase before an earthquake ruptures. In this study, constant η is considered for each
214 case.

215 Some authors (Knopoff et al., 1973; Cohen, 1979; Rice, 1993; Xu and Knopoff,
216 1994; Knopoff and Ni, 2001; Bizzarri, 2012a; Dragoni and Santini, 2015) considered
217 that viscosity plays a role on causing seismic radiation to release strain energy during
218 faulting.

219

220 **3 Normalization of Equation of Motion**

221 Putting Eq. 2 and $\Phi=\eta v$ into Eq. 1 leads to

222

$$223 \quad m d^2 u / dt^2 = -K(u - v_p t) - F_0 \exp(-u/u_c) - \eta v. \quad (3)$$

224

225 Eq. 3 is normalized for easy numerical computations based on the normalization
 226 parameters, which is dimensionless: $D_o=F_o/K$, $\omega_o=(K/m)^{1/2}$, $\tau=\omega_o t$, $U=u/D_o$, and
 227 $U_c=u_c/D_o$. The normalized velocity, acceleration, and driving velocity are $V=dU/d\tau=$
 228 $[F_o/(mK)^{1/2}]^{-1}du/dt$, $A=d^2U/d\tau^2=(F_o/m)^{-1}d^2u/dt^2$, and $V_p=v_p/(D_o\omega_o)$, respectively.
 229 Define $\Omega=\omega/\omega_o$ to be the dimensionless angular frequency, and thus the phase ωt
 230 becomes $\Omega\tau$. For the purpose of simplification, $\eta/(mK)^{1/2}$ is denoted by η below.
 231 Substituting all normalization parameters into Eq. 3 leads to

232

$$233 \quad d^2U/d\tau^2=-U-\eta dU/d\tau-\exp(-U/U_c)+V_p\tau. \quad (4)$$

234

235 In order to numerically solve Eq. (4), we define two new parameters, i.e., $y_1=U$ and
 236 $y_2=dU/d\tau$. Eq. 4 can be re-written as two first-order differential equations:

237

$$238 \quad dy_1/d\tau=y_2 \quad (5a)$$

239

$$240 \quad dy_2/d\tau=-y_1-\eta y_2-\exp(-y_1/U_c)+V_p\tau. \quad (5b)$$

241

242 We can numerically solve Eq. 5 by using the fourth-order Runge-Kutta method (Press
 243 et al., 1986). In general, the values of D_o are several meters and ω_o are in the range of
 244 0.1 Hz to few Hz (see Wang, 2016). This leads to that $D_o\omega_o$ has an order of
 245 magnitude of 1 m/s. The value of V_p must be much smaller than 1 because of $v_p\approx 10^{-10}$
 246 m/s. Since the value of V_p mainly influences the recurrence time, T_R , between two
 247 events and can only make a very small influence on the pattern of time variations in
 248 velocities and displacements of events. In order to study long-term earthquake
 249 recurrence, there must be numerous modeled events with clear and visualized time

250 functions of displacements and velocities for an event in the computational time
251 period. If $V_p=10^{-10}$ is considered, T_R is very long and thus τ_D is much shorter than T_R .
252 This makes the time function of an event displayed in the long-term temporal
253 variation in slip looks like just a step function for the displacements and an impulse
254 for the velocities. Hence, in order to get fine visualization a larger value of V_p is
255 necessary. The value of $V_p\tau$ is usually very small during an event and cannot
256 influence the rupture because of a very tiny value of V_p . Numerical test shows that
257 when $V_p>10^{-2}$, the value of $V_p\tau$ is not small during an event and can influence the
258 rupture. Hence, $V_p=10^{-2}$ is taken in this study. The backward slip is not allowed in the
259 simulations, because of common behavior of forward earthquake ruptures.

260 A phase portrait, which is a plot of a physical quantity, y , versus another, x , i.e.,
261 $y=f(x)$, is commonly used to represent nonlinear behavior of a dynamical system
262 (Thompson and Stewart, 1986). The intersection point between $f(x)$ and the bisection
263 line of $y=x$, is defined as the fixed point, that is, $f(x)=x$. If $f(x)$ is continuously
264 differentiable in an open domain near a fixed point x_f and $|f'(x_f)|<1$, attraction can
265 appear at the fixed point. Chaos can also be generated at some attractors. The details
266 can be seen in Thompson and Stewart (1986). In this study, the phase portrait is the
267 plot of V/V_{max} versus U/U_{max} .

268

269 **4 Simulation Results**

270 Numerical simulations lead to the temporal variations in particle velocities and
271 displacements as displayed in Fig. 1. The values of V_m and D , respectively, represent
272 the peak value of velocity and final slip for each event. Since four cases related to our
273 values of a particular model parameter, there are four values of V_m and D in a figure.

274 In order to plot the temporal variations in both normalized displacements and
 275 velocities, the maximum values of V_m and D of the modelled events, i.e., V_{max} and
 276 U_{max} , respectively, are taken into account. The values of V_m and D usually appear in
 277 the panel marked by “a” of a figure. Simulation results are shown in Figs. 4–12. The
 278 temporal variations in V/V_{max} (displayed by thin solid lines) and cumulative slip
 279 $\Sigma U/U_{max}$ (displayed by solid lines) are displayed in the left-handed-side panels. The
 280 normalization scales to plot the temporal variations in slip and velocity are V_{max} for
 281 the velocities and the final value of $\Sigma U/U_{max}$ for the displacements in the
 282 computational time. Hence, the upper bound scale is “1” for the two temporal
 283 variations. Hence, only the patterns of temporal variations of velocity and cumulative
 284 slip are concerned in these figures.

285 Simulation results displayed in these figures show that the maximum values of both
 286 V and U decrease from case (a) to case (d) in each figure. Hence, the maximum
 287 velocity and maximum displacement, which are denoted by V_{max} and U_{max} ,
 288 respectively, for case (a) can be taken as the scaled factor to normalize the waveforms
 289 from case (a) to case (d). This makes us easily to compare the waveforms of the four
 290 cases in each figure.

291 The cases excluding the viscous effect, i.e., $\eta=0$, are first simulated and results are
 292 shown in Fig. 4 for four values of U_c : (a) for $U_c=0.2$; (b) for $U_c=0.4$; (c) for $U_c=0.8$;
 293 and (d) for $U_c=1.0$. The results of the cases including viscosity, i.e., $\eta \neq 0$, are
 294 displayed in Figs. 5–7 for four values of η : (a) for $\eta=0.20$; (b) for $\eta=0.40$; (c) for
 295 $\eta=0.6$; and (d) for $\eta=0.8$. The values of U_c are 0.2 in Fig. 5, 0.5 in Fig. 6, and 0.8 in
 296 Fig. 7.

297 The left-handed-side panels in Fig. 4 with $\eta=0$ show that the peak velocity of an
 298 event, V_m , and final slip, D , with the respective maximum values in case (a) as

299 mentioned above, for all simulated events decrease with increasing U_c . From Fig. 3,
 300 the force drop, ΔF , decreases with increasing U_c for a certain final slip, thus
 301 indicating that larger ΔF yields higher V_m and larger D . This interprets the negative
 302 dependence of V_m and D on U_c . When the viscous effect is absent, i.e., $\eta=0$, the value
 303 of τ_D increases with U_c ; while T_R decreases with increasing U_c . When $U_c=1$, V_m and
 304 D are both very small and the system behaves like creeping of a fault. In the
 305 right-handed-side panels, there are two fixed points for each case: one is called the
 306 non-zero fixed point at larger V and larger U and the other the zero fixed point at $V=0$
 307 and $U=0$. The slope at a fixed point is defined to be $d(V/V_{\max})/d(U/U_{\max})=$
 308 $(U_{\max}/V_{\max})(dV/dU)$. The absolute values of slope at the two fixed points decrease
 309 with increasing U_c , thus suggesting that the fixed point is not an attractor for small U_c
 310 and could be an attractor for larger U_c . The phase portrait for $U_c=1$ is very tiny,
 311 because the final slip for $U_c=1.0$ is much smaller than those for $U_c=0.2, 0.4,$ and 0.8 .
 312 Hence, $U_c=1$ will not be taken into account in the following simulations.

313 The left-handed-side panels in Figs. 5–7 show that V_m and D decrease when either
 314 U_c or η increases; while τ_D increases with η and U_c . Meanwhile, T_R increases when
 315 either η increases or U_c decreases. The right-handed-side panel exhibits that the
 316 phase portraits are coincided for all simulated events for a certain η . The absolute
 317 values of slope at the two fixed points decrease when either U_c or η increases. This
 318 suggests that the fixed point is not an attractor for small U_c and low η , and can be an
 319 attractor for large U_c and high η . Like Fig. 4, the final slip decreases with increasing
 320 U_c .

321 From Figs. 5–7, we can see that the temporal variation in cumulative slip can be
 322 described by the perfectly periodic model as mentioned above. Hence, when U_c and η
 323 do not change with time, the rate of cumulative slip retains a constant in the

324 computational time period. This is similar to the simulation results with the periodical
325 earthquake occurrences obtained by some authors (e.g., Rice and Tse, 1986; Ryabov
326 and Ito, 2001; Erickson et al., 2008; Mitsui and Hirahara, 2009) based on the
327 one-body model with rate- and state-dependent friction or velocity- weakening
328 friction. But, the present result is inconsistent with the simulation results, from which
329 either the time-predictable model or the slip-predictable model cannot interpret the
330 temporal variation in cumulative slip, based on the same model obtained by others
331 (e.g., He et al., 2003; Bazzarri 2012b; Bizzarri and Crupi, 2014; Kostić et al., 2013a,b;
332 Franović et al., 2016). The differences between the two groups of researchers might
333 be due to distinct additional constrains in respective studies. Although the detailed
334 discussion of such differences is important and significant, it is out of the scope of this
335 study and ignored here.

336 The phase portraits in Figs. 5–7 exhibit two kinds of fixed points as mentioned
337 above. The absolute values of slope at the non-zero fixed point are higher than 1 and
338 decreases with increasing η . This means that larger η is easier to generate an attractor
339 than small η . However, the reducing rate of absolute value of slope decreases with
340 increasing U_c . The absolute values of slope of the zero fixed point are higher than 1
341 and decrease with increasing η . This suggests that the zero fixed points can be an
342 attractor. This behavior becomes weaker when U_c increases.

343 Figs. 4–7 show that when U_c and η are constants during the computational time
344 periods, the general patterns of temporal variations in cumulated slip do not change.
345 Some of the previous studies (e.g., Bizzarri, 2012a,b; and Franović et al., 2016)
346 suggest that the patterns of temporal variations in cumulated slip can change with
347 time. The changes of U_c and η with time should play the main roles. From
348 $u_c = \rho_f C_v h / \mu_f \Lambda$ of the TP model (see Rice 2006), the width of the slipping zone, h ,

349 where the maximum deformation is concentrated (Bizzarri, 2009), is a significant
 350 parameter in this study. From geological surveys, Rathbun and Marone (2010)
 351 observed that h is not spatially uniform even within a single fault. Hull (1988) and
 352 Marrett and Allmendinger (1990) found that the wear processes occurring during
 353 faulting could widen h , and thus h could vary with time. According to the results
 354 gained by several authors (e.g., Power et al., 1988; Robertson, 1983; and Bizzarri,
 355 2010), Bizzarri (2012b) proposed a linear dependence of h on the cumulated slip,
 356 $S(t)=\sum D(t)$, i.e., $h(t)=CS(t)$ where C is a dimensionless increasing rate of h with S and
 357 is considered to be a constant in each case. Based on $h(t)=CS(t)$, the more mature the
 358 fault is, the thicker its slip zone is. Since u_c is proportional to h and $U_c=u_c/D_o$, U_c is
 359 related to C . Here, we assume that U_c varies with cumulative slip in the following
 360 way: $U_c=U_{co}+C\sum U(t)$ where U_{co} is the initial value of U_c . Simulation results for four
 361 values of C are shown in Figs. 8–12: (a) for $C=0.0001$; (b) for $C=0.001$; (c) for
 362 $C=0.01$; and (d) for $C=0.05$ when $\eta=0$ in Figs. 8–10; (a) for $C=0.0001$; (b) for
 363 $C=0.001$; (c) for $C=0.01$; and (d) for $C=0.038$ when $\eta=1$ in Fig. 11; and (a) for
 364 $C=0.0001$; (b) for $C=0.001$; (c) for $C=0.01$; and (d) for $C=0.0136$ when $\eta=1$ in Fig. 12.
 365 The initial values of U_c are: 0.1 for Fig. 8, 0.5 for Fig. 9, 0.9 for Fig. 10, 0.1 for Fig.
 366 11, and 0.5 for Fig. 12. Note that the value U_c varies with time due to time-varying h .

367 The left-handed-side panels of Figs. 8–12 show that V_m , D , τ_D , and T_R are all
 368 similar when $C\leq 0.001$. However, in general V_m and D decrease with increasing C ; T_R
 369 slightly decreases with increasing C ; and τ_D slightly increases with C . A decrease in D
 370 is particularly remarkable when $C\geq 0.01$. When h is wider than a critical value with
 371 $C=0.05$ for $\eta=0$, normal earthquakes cannot occur and only creeping may happen.
 372 The critical value of h decreases when the viscous effect is present with $\eta=1$ in this
 373 study. This decrease is also influenced by U_c : $C=0.038$ when the initial value of U_c is

374 0.1 and $C=0.0136$ when the initial value of U_c is 0.5. Obviously, T_R decreases with
375 increasing C , thus leading to a decrease in T_R with increasing h . This is similar to the
376 result obtained by Bizzarri (2010; 2012b). But, the viscous effect was not included in
377 his studies.

378 The right-handed-side panels of Figs. 8–12 exhibit that the phase portraits for
379 $C=0.001$ are slightly different from those for $C=0.0001$ even though the patterns of
380 their variations in V and U are similar; while the phase portraits for $C>0.001$ are
381 different from those for $C\leq 0.001$. An increase in h due to an increase in C with
382 cumulative slip enlarges U_c . This can be explained from Fig. 3 which shows that
383 larger U_c yields a lower ΔF than smaller U_c for the same final slip. Hence, an increase
384 in U_c produces a decrease in ΔF , thus resulting in low V_m and small D . In addition,
385 An increase in U_c makes $\exp(-U/U_c)$ approach unity, especially for small U , thus
386 reducing the nonlinear effect caused by TP friction.

387 Unlike Figs. 4–7, the size of phase portraits in the right-handed-side panels of Figs.
388 8–12 decreases with increasing C . This reflects a decrease in both T_R and D of events
389 with increasing C as mentioned previously. The absolute values of slope at the
390 non-zero fixed point are higher than 1 and only slightly decrease with time when
391 $C<0.01$; while the values remarkably decrease with time when $C\geq 0.01$. The absolute
392 values of slope at the zero fixed point are higher than 1 and only slightly decrease
393 with time when $C<0.01$; while those decrease with time when $C\geq 0.01$. Results
394 suggest that the non-zero fixed points for all cases in study are not an attractor; and
395 those at the zero fixed points can evolve to an attractor with time when $C\geq 0.01$. The
396 phenomenon is particularly remarkable for $C=0.05$ in Figs. 8–10, $C=0.0380$ in Fig. 11,
397 and $C=0.0136$ in Fig. 12, and the evolution is faster for large U_c than for small U_c .

398

399 **5 Discussion**

400 The simulation results as mentioned previously demonstrate that when U_c and η are
401 constants during the computational time periods, the general patterns of temporal
402 variations in cumulated slip cannot change. In order to investigate the effect of
403 time-varying η and U_c on the patterns of temporal variations in cumulated slip, we
404 must consider changes of U_c and η with time. The viscosity coefficient can actually
405 vary immediately before and after the occurrence of an earthquake (see Spray, 1883,
406 2005; Wang, 2017b,c). But, a lack of long-term variation in η does not allow us to
407 explore its possible effect on the change of general patterns of temporal variations in
408 cumulated slip. Here, only the possible effect due to time-varying U_c .

409 As mentioned above, the equality $U_c = u_c / D_o$ leads to $U_c = \rho_f C_v h / \mu_f D_o \Lambda$. Obviously,
410 U_c is controlled by six factors, i.e., ρ_f , C_v , h , μ_f , D_o , and Λ . Since the tectonics of a
411 region is generally stable during a long time, the value of $D_o = F_o / K$ could not change
412 too much and thus would not influence U_c . The Debye law (cf. Reif, 1965) gives
413 $C_v \sim (T + 273.16)^3$, where 273.16 is the value to convert temperature from Celsius to
414 Kelvin, at low T and $C_v \approx \text{constant}$ at high T . The threshold temperature, from which C_v
415 begins to approach a constant, is 200–300 °K. In this study, C_v is almost a constant
416 because of $T > 250$ °C = 523.16 °K, which is the average ambient temperature of fault
417 zone with depths ranging from 0 to 20 km. Hence, C_v is almost constant during a long
418 time and thus cannot influence U_c .

419 The frictional strength, μ_f , is influenced by several factors including humidity,
420 temperature, sliding velocity, strain rate, normal stress, thermally activated rheology
421 etc (Marone, 1998; Rice, 2006), and thus can change with time (Sibson, 1992; Rice,
422 2006). Hirose and Bystricky (2007) observed that serpentine dehydration and

423 subsequent fluid pressurization due to co-seismic frictional heating may reduce μ_f and
424 thus promote further weakening in a fault zone. The pore fluid pressure exists in wet
425 rocks, yet not in dry rocks. Clearly, the time variation in μ_f can affect the earthquake
426 recurrences. However, a lack of long-term observations of μ_f during a seismic cycle
427 makes the studies of its effect on earthquake recurrence be impossible.

428 The fluid density ρ_f and the porosity n depend on T and p . Although there are
429 numerous studies on such dependence (Lachenbruch, 1980; Bizzarri, 2012b; and cited
430 references therein), observed data and theoretical analyses about the values of ρ_f and n
431 during a seismic cycle are rare.

432 The porosity is associated with the permeability, κ . Bizzarri (2012c) pointed out
433 that the time-varying permeability, $\kappa(t)$, and porosity of a fault zone (cf. Mitsui and
434 Cocco, 2010; Bizzarri, 2012b) can reduce T_R . One of the Kozeny–Carman's (KC)
435 relations (Costa, 2006; and references cited therein) is: $\kappa(t) = \kappa_C \phi^2(t) d^3(t) / [1 - \phi(t)]^2$,
436 where κ_C is a dimensionless constant depending on the material in consideration; ϕ is
437 V_{voids} / V_{tot} where V_{voids} and V_{tot} are, respectively, the pore volume and the total volume
438 of the porous materials; and d is the (average) diameter of the grains, ranging between
439 4×10^{-5} m and 1×10^{-4} m (Niemeijer et al., 2010). Usually, κ , ϕ , and d can vary in the
440 fault zone (Segall and Rice, 1995). After faulting κ and ϕ would change and d
441 becomes smaller because of refining of the grains. According to this relation, Bizzarri
442 (2012b) found that $\kappa(t)$ could significantly reduce T_R in comparison with the base
443 model with constant κ . The reason is explained below. An increase in permeability
444 can result in an increase in pore pressure, p_f . This can reduce the frictional resistance
445 from $\tau = \mu(\sigma_n - p_f)$ and thus could trigger earthquakes earlier. Hence, the time-varying
446 permeability can change T_R . Nevertheless, we cannot investigate its influence on

447 earthquake recurrence here because there is a lack of a long-term observation of
448 hydraulic parameters during a seismic cycle.

449 It is significant to explore the factors that can yield a non-perfectly periodic seismic
450 cycle. The width of the slipping zone, h , can be a candidate as pointed out by some
451 authors (e.g., Bizzarri, 2009; Rathbun and Marone, 2010). Since the displacement
452 along a fault is controlled by the fault rheology, h should depend on the rheology on
453 the sliding interface. The wear processes occurring during faulting could widen h
454 (Hull, 1988; Marrett and Allmendinger, 1990). According to the results gained by
455 several authors (e.g., Power et al., 1988; Robertson, 1983; and Bizzarri, 2010),
456 Simulation results for various values of C and the results are shown in Figs. 8–10 with
457 $\eta=0$ and in Figs. 11–12 with $\eta=1$. Results exhibit that when $C>0.0001$, the wear
458 process affects the recurrence of slip and the effect increases with C and when C is
459 larger than an upper-bound value, larger-sized events cannot occur and the earthquake
460 recurrence does not exist. Both T_R and D decrease when the fault becomes more
461 mature due to a thicker slip zone. Meanwhile, the viscous effect can also play a
462 secondary role on the earthquake recurrence because it makes upper-bound value
463 become smaller. Although either the time- or slip-predictable model can describe the
464 temporal variations of cumulative slip of events occurring in the earlier time period,
465 they cannot interpret those of events in the later parts. This might suggest that it is
466 more difficult to produce large earthquakes along a fault when it becomes more
467 mature, especially for the cases with viscosity. This implicates that seismic hazard is
468 higher for a young fault than a mature one. Hence, it is significant and important to
469 identify the width of slip zone of an earthquake fault for seismic hazard estimates.

470

471 **6 Conclusions**

472 To study the frictional and viscous effects on earthquake recurrence, numerical
473 simulations of the temporal variations in cumulative slip have been conducted based
474 on the normalized equation of a one-body model in the presence of thermal-
475 pressurized slip-weakening friction and viscosity. The wear process, which is included
476 in the friction law, is also taken into account. The model parameters of friction and
477 viscosity are represented, respectively, by U_c and η , where $U_c = u_c/D_o$ is the normalized
478 characteristic distance and η is the normalized damping coefficient. Numerical
479 simulation of the time variations in V/V_{max} and cumulative slip $\Sigma U/U_{max}$, and the phase
480 portrait of V/V_{max} versus U/U_{max} are made for various values of U_c and η .

481 Results exhibit that both friction and viscosity remarkably affect earthquake
482 recurrences. The recurrence time, T_R , increase when η increases or U_c decreases. The
483 final slip, D , and the duration time of slip, τ_D , of an event slightly decrease when η or
484 τ_D increases and slightly increases with U_c . Considering the effect due to wear process,
485 the thickness of slip zone, h that depends on the cumulated slip, $S(t) = \Sigma D(t)$, i.e.,
486 $h(t) = CS(t)$ (C =a dimensionless constant), is an important factor in influencing
487 earthquake recurrences. U_c increases with ΣU with an increasing rate of C . When
488 $C > 0.0001$, the wear process influences the recurrence of slip and the effect increases
489 with C . When C is larger than an upper-bound value, larger-sized events cannot occur
490 and the earthquake recurrence does not exist. If the slip zone becomes thicker, the
491 fault is more mature. This makes T_R and D become shorter. This might suggest that it
492 is more difficult to produce large earthquakes along a fault when it becomes more
493 mature. This phenomenon becomes remarkable when the viscous effect exists because
494 the upper-bound value becomes smaller. The temporal variation in slip cannot be
495 interpreted by the time-predictable or slip-predictable model when the fault is affected
496 by wear process with large C . In addition, the size of phase portrait of V/V_{max} versus

497 U/U_{max} decreases with increasing C . This again reflects decreases in both T_R and D of
498 events with increasing C as inferred from the temporal variations in cumulative slip.

499

500 **Acknowledgments** The author would like to thank Prof. Filippos Vallianatos
501 (Editor of NHESS) and two anonymous reviewers for their valuable comments and
502 suggestions to help me to substantially improve this article. The study was financially
503 supported by Academia Sinica and the Ministry of Science and Technology (Grant
504 No.: MOST-106-2116-M-001-005).

505

506 **References**

507 Abaimov, S.G., Turcotte D.L., Shcherbakov R., and Rundle J.B.: Recurrence and
508 interoccurrence behavior of self-organized complex phenomena, *Nonlin.*
509 *Processes Geophys.*, 14, 455-464, 2007

510 Abe, Y. and Kato N.: Complex earthquake cycle simulations using a two-degree-
511 of-freedom spring-block model with a rate- and state-friction law, *Pure. Appl.*
512 *Geophys.*, 170, 745-765, 2013.

513 Ando, M.; Source mechanisms and tectonic significance of historic earthquakes along
514 the Nankai trough, Japan, *Tectonophys.*, 27, 119-140, 1975

515 Bakun, W.H. and McEvilly T.V.: Earthquakes near Parkfield, California: comparing
516 the 1934 and 1966 sequences, *Science*, 205, 1375-1377, 1979.

517 Bakun, W.H. and McEvilly T.V.: Recurrence models and Parkfield, California,
518 earthquakes, *J. Geophys. Res.*, 89, 3051-3058, 1984.

519 Beeler, N.M., Lockner D.L., and Hickman S.H.: A simple stick-slip model for
520 repeating earthquakes and its implication for microearthquakes at Parkfield, *Bull.*
521 *Seism. Soc. Am.*, 91(6), 1797-1804, 2001.

522 Belardinelli, M.E. and Belardinelli E.: The quasi-static approximation of the
523 spring-slider motion. *Nonl. Processes Geophys.*, 3, 143-149, 1996.

524 Bizzarri, A.: What does control earthquake ruptures and dynamic faulting? A review
525 of different competing mechanism, *Pure. Appl. Geophys.*, 166, 741-776, 2009.

526 Bizzarri. A.: On the recurrence of earthquakes: Role of wear in brittle faulting,
527 *Geophys. Res., Letts.*, 37, L20315, <http://dx.doi.org/10.1029/2010GL045480>,
528 2010.

529 Bizzarri, A.: Modeling repeated slip failures on faults governed by slip- weakening
530 friction, *Bull. Seism. Soc. Am.*, 102(2), 812-821 doi:10.1785/0120110141, 2012a.

531 Bizzarri, A.: What can physical source models tell us about the recurrence time of
532 earthquakes?, *Earth-Sci. Rev.*, 115, 304-318 <http://dx.doi.org/10.1016/j.earscirev>.
533 2012.10.004, 2012b

534 Bizzarri., A.: Effects of permeability and porosity evolution on simulated earthquakes,
535 *J. Struct. Geol.*, 38, 243-253, <http://dx.doi.org/10.1016/j.jsg.2011.07.009>, 2012c

536 Bizzarri, A. and Crupi P.: Linking the recurrence time of earthquakes to source
537 parameters: A dream or a real possibility?, *Pure. Appl. Geophys.*, 171, 2537-2553,
538 DOI:10.1007/s00024-013-0743-1, 2014.

539 Brun, J.L. and Gomez A.B.: A four-parameter, two degree-of-freedom block-spring
540 model: Effect of the driver velocity, *Pure. Appl. Geophys.*, 143(4), 633-653, 1994.

541 Burridge, R. and Knopoff L.: Model and theoretical seismicity, *Bull. Seism. Soc. Am.*,
542 57, 341-371, 1967.

543 Byerlee, J.D.: Brittle-ductile transition in rocks, *J. Geophys. Res.*, 73, 4711-4750,
544 1968.

545 Carlson, J.M. and Langer J.S: Mechanical model of an earthquake fault, *Phys. Rev. A*,
546 40, 6470-6484, 1989.

547 Chen, K.H., Nadeau R.M., and Rau R.J.: Towards a universal rule on the recurrence
548 interval scaling of repeating earthquakes?, *Geophys. Res., Letts.*, 34, L16308,
549 doi:10.1029/2007GL030554, 2007.

550 Cohen, S.: Numerical and laboratory simulation of fault motion and earthquake
551 occurrence, *Rev. Geophys. Space Phys.*, 17(1), 61-72, 1979.

552 Costa, A.: Permeability-porosity relationship: a reexamination of the Kozeny–
553 Carman equation based on a fractal pore-space geometry assumption, *Geophys.*
554 *Res. Letts.*, 33, L02318 <http://dx.doi.org/10.1029/2005GL025134>, 2006.

555 Davis, P.M., Jackson D.D., and Kagan Y.Y.: The longer it has been since the last
556 earthquake, the longer the expected time till the next?, *Bull. Seism. Soc. Am.*,
557 79:1439-1456, 1989.

558 Dragoni, M. and Piombo A.: Dynamics of a seismogenic fault subject to variable
559 strain rate, *Nonlin. Processes Geophys.*, 18, 431-439, doi:10.5194/npg-18-431-
560 2011, 2011.

561 Dragoni, M. and Santini S.: A two-asperity fault model with wave radiation,
562 *Phys. Earth Planet. Inter.*, 248, 83-93, 2015.

563 Enescu, B., Struzik Z., and Kiyono K.: On the recurrence time of earthquakes: insight
564 from Vrancea (Romania) intermediate-depth events, *Geophys. J. Int.*, 172, 395-
565 404, doi:10.1111/j.1365-246X.2007.03664.x, 2008.

566 Erickson, B., Birnir B., and Lavall´ee D.: A model for aperiodicity in earthquakes,
567 *Nonlin. Processes Geophys.*, 15, 1-12, 2008.

568 Erickson, B., Birnir B., and Lavall´ee D.: Periodicity, chaos and localization in a
569 Burridge–Knopoff model of an earthquake with rate-and-state friction, *Geophys.*
570 *J. Int.*, 187, 178-198, doi:10.1111/j.1365-246X.2011.05123.x, 2011.

571 Franovic´, I., Kostic´ S., Perc M., Klinshov V., Nekorkin V., and Kurths J.: Phase
572 response curves for models of earthquake fault dynamics, *Chaos*, 26, 063105,
573 <http://dx.doi.org/10.1063/1.4953471>, 2016.

574 Hasumi, T.: Interoccurrence time statistics in the two-dimensional Burridge- Knopoff
575 earthquake model, *Phys. Rev. E*, 76, 026117, DOI:10.1103/PhysRevE.76.026117,
576 2007.

577 He, C., Wong T.f., and Beeler N.M.: Scaling of stress drop with recurrence interval
578 and loading velocity for laboratory-derived fault strength relations, *J. Geophys.*
579 *Res.*, 108(B1), 2037 doi:10.1029/2002JB001890, 2003.

580 Hirose, T. and Bystricky M.: Extreme dynamic weakening of faults during
581 dehydration by coseismic shear heating, *Geophys. Res., Letts.*, 34, L14311
582 doi:10.1029/2007GL030049, 2007.

583 Huang, J. and Turcotte D.L.: Are earthquakes an example of deterministic chaos?,
584 *Geophys. Res., Letts.*, 17(3), 223-226, 1990.

585 Huang, J. and Turcotte D.L.: Evidence of chaotic fault interactions in the seismicity of
586 the San Andreas fault and Nankai trough, *Nature*, 348, 234-236, 1992.

587 Hudson, J.A.: The excitation and propagation of elastic waves. Cambridge
588 Monographs on Mechanics and Applied Mathematics, Cambridge Univ. Press,
589 226 pp., 1980.

590 Hull, J.: Thickness–displacement relationships for deformation zones, *J. Struct. Geol.*,
591 10, 431-435, [http://dx.doi.org/10.1016/0191-8141\(88\)90020-X](http://dx.doi.org/10.1016/0191-8141(88)90020-X), 1988.

592 Jeffreys, H.: On the mechanics of faulting, *Geol. Mag.*, 79, 291, 1942.

593 Kanamori, H. and Allen C.R.: Earthquake repeating time and average drop, In: Das et
594 al. (eds.) *Earthquake Source Mechanics Maurice Ewing Series 6*, AGU, 227-235,
595 1986.

596 Kittel C, Knight WD, Ruderman MA (1968) *Mechanics*. Berkeley Physics Course vol
597 1 McGraw-Hill Book Co New York, 1986.

598 Knopoff, L., and Ni X.X.: Numerical instability at the edge of a dynamic fracture,
599 *Geophys. J. Int.*, 147, F1-F6, 2001.

600 Knopoff, L., Mouton J.Q., and Burridge R.: The dynamics of a one-dimensional fault
601 in the presence of friction, *Geophys. J. R. astro. Soc.*, 35, 169-184, 1973.

602 Kostić, S., Franović I., Todorović K., and Vasović N.: Friction memory effect in
603 complex dynamics of earthquake model, *Nonlin. Dyn.* 73, 1933-1943, DOI:10.
604 1007/s11071-013-0914-8, 2013a.

605 Kostić, S., Vasović N., Franović I., and Todorović K.: Dynamics of simple earthquake
606 model with time delay and variation of friction strength, *Nonlin. Processes*
607 *Geophys.*, 20, 857-865, doi:10.5194/npg-20-857-2013, 2013b.

608 Lachenbruch, A.H.: Frictional heating, fluid pressure, and the resistance to fault
609 motion, *J. Geophys. Res.*, 85, 6097-6122, 1980.

610 Lapusta, N. and Rice J.R.: Nucleation and early seismic propagation of small and
611 large events in a crustal earthquake model, *J. Geophys. Res.*, 108, 1-18, 2003.

612 Marone, C.: Laboratory-derived friction laws and their application to seismic faulting,
613 *Ann. Rev. Earth Planet. Sci.*, 26, 643-669, 1998.

614 Marrett, R. and Allmendinger R.W.: Kinematic analysis of fault-slip data, *J. Struct.*
615 *Geol.*, 12, 973-986, doi.org/10.1016/0191-8141(90)90093-E, 1990.

616 Mitsui, Y. and Cocco M.: The role of porosity evolution and fluid flow in frictional
617 instabilities: a parametric study using a spring-slider dynamic system, *Geophys.*
618 *Res., Letts.*, 37, L23305, doi.org/10.1029/2010GL045672, 2010.

619 Mitsui, Y. and Hirahara K.: Coseismic thermal pressurization can notably prolong
620 earthquake recurrence intervals on weak rate and state friction faults: numerical

621 experiments using different constitutive equations, *J. Geophys. Res.*, 114,
622 B09304, doi.org/10.1029/2008JB006220, 2009.

623 Murray, J. and Segall P.: Testing time-predictable earthquake recurrence by direct
624 measurement of strain accumulation and release, *Nature*, 49, 287-291, 2002.

625 Nadeau, R.M. and Johnson L.R.: Seismological studies at Parkfield VI moment
626 release rates and estimates of source parameters for small repeating earthquake,
627 *Bull. Seism. Soc. Am.*, 88, 790-814, 1998.

628 Niemeijer, A., Marone C., and Ellsworth D.: Frictional strength and strain weakening
629 in simulated fault gouge: competition between geometrical weakening and
630 chemical strengthening, *J. Geophys. Res.*, 115, B10207, doi.org/10.1029/
631 2009JB000838, 2010.

632 Nur, A.: Nonuniform friction as a physical basis for earthquake mechanics, *Pure. Appl.*
633 *Geophys.*, 116, 964-989, 1978.

634 Okada, T., Matsuzawa T., and Hasegawa A.: Comparison of source areas of
635 M4.8+/-0.1 repeating earthquakes off Kamaishi, NE Japan: are asperities
636 persistent features?, *Earth Planet. Sci. Letts.*, 213(3-4), 361-374, doi.org/
637 10.1016/S0012-821X(03000299-1), 2003.

638 Power, W.L., Tullis T.E., and Weeks D.J.: Roughness and wear during brittle faulting,
639 *J. Geophys. Res.*, 93, B12, 15268-15278, doi.org/10.1029/JB093iB12p15268,
640 1988.

641 Press, WH., Flannery B.P., Teukolsky S.A., and Vetterling W.T.: *Numerical Recipes*,
642 Cambridge Univ. Press Cambridge, 1986.

643 Rathbun, A.P. And Marone C.: Effect of strain localization on frictional behavior of
644 sheared granular materials, *J. Geophys. Res.*, 115, B01204 doi.org/10.1029/
645 2009JB006466, 2010.

646 Reid, H.F.: The California earthquake of April 18, 1906, In: Report of the State
647 Investigation Commission 2, Mechanics of the Earthquake Carnegie Inst
648 Washington, D.C., 1910.

649 Reif, F.: Fundamentals of statistical and thermal physics, McGraw-Hill, New York,
650 651 pp., 1965.

651 Rice, J.R.: Spatio-temporal complexity of slip on a fault, *J. Geophys. Res.*, 98, B6,
652 9885-9907, 1993.

653 Rice, J.R.: Heating and weakening of faults during earthquake slip, *J. Geophys. Res.*,
654 111, B05311, doi:10.1029/2005JB004006, 2006.

655 Rice, J.R. and Tse S.T.: Dynamic motion of a single degree of freedom system
656 following a rate and state dependent friction law, *J. Geophys. Res.*, 91, B1,
657 521-530, 1986.

658 Rice, J.R., Lapusta N., and Ranjith K.: Rate and state dependent friction and the
659 stability of sliding between elastically deformable solids, *J. Mech. Phys. Solids*,
660 49, 1865-1898, 2001.

661 Robertson, E.C.: Relationship of fault displacement to gouge and breccia thickness,
662 *Mining Engin.*, 35, 1426-1432, 1983.

663 Rubinstein, J.L., Ellsworth W.L., Beeler N.M., Kilgore B.D., Lockner D.A., and
664 Savage H.M.: Fixed recurrence and slip models better predict earthquake
665 behavior than the time- and slip-predictable models: 2. Laboratory earthquakes, *J.*
666 *Geophys. Res.*, 117, B02307, doi:10.1029/2011JB008723, 2012.

667 Ryabov, V.B. and Ito K.: Intermittent phase transitions in a slider-spring model as a
668 mechanism for earthquakes, *Pure. Appl. Geophys.*, 158:919-930, 2001.

669 Scholz, C.H.: *The Mechanics of Earthquakes and Faulting*. Cambridge Univ. Press
670 Cambridge, 439 pp., 1990.

671 Schwartz, D.P. and Coppersmith K.S.: Fault behavior and characteristic earthquakes:
672 examples from the Wasatch and San Andreas fault zones, *J. Geophys. Res.*, 89,
673 5681-5698, 1984.

674 Segall, P. and Rice J.R.: Dilatancy, compaction, and slip instability of a
675 fluid-infiltrated fault, *J. Geophys. Res.*, 100, 22155-22171, 1995.

676 Shimazaki, K. and Nakata T.: Time-predictable model for large earthquakes, *Geophys.*
677 *Res. Letts.*, 7, 279-282, doi.org/10.1029/GL007i004p00279, 1980.

678 Sibson, R.H.: Interaction between temperature and pore-fluid pressure during
679 earthquake faulting and a mechanism for partial or total stress release, *Natural*
680 *Phys. Sci.*, 243, 66-68, 1973.

681 Sibson, R.H.: Implications of fault-valve behavior for rupture nucleation and
682 recurrence, *Tectonophys.*, 211,283-293, 1992.

683 Sieh, K.: A review of geological evidence for recurrence times of large earthquakes,
684 In: *Earthquake Prediction—An International Review*, Maurice Ewing Series, 4,
685 AGU, 181-207, 1981.

686 Sieh, K., Natawidjaja D., Meltzner A.J., Shen C.C., and Cheng H.: Earthquake
687 supercycles inferred from sea-level changes recorded in the corals of West
688 Sumatra, *Science*, 322, 1674-1678, 2008.

689 Sykes, L.R. and Quittmeyer R.C.: Repeat times of great earthquakes along simple
690 plate boundaries, In: *Earthquake Prediction—An International Review*, Maurice
691 Ewing Series 4, AGU, 217-247, 1981.

692 Spray, J.G.: Viscosity determinations of some frictionally generated silicate melts:
693 Implications for fault zone rheology at high strain rates, *J. Geophys. Res.*, 98, B5,
694 8053-8068, 1983.

695 Spray, J.G.: Evidence for melt lubrication during large earthquakes, *Geophys. Res.*,

696 Letts., 32, L07301, doi:10.1029/2004GL022293, 2005.

697 Sykes, L.R. and Menke W.: Repeat times of large earthquakes: implications for
698 earthquake mechanics and long-term prediction, *Bull. Seism. Soc. Am.*, 96(5),
699 1569-1596, doi.org/10.1785/0120050083, 2006.

700 Thompson., J.M.T. and Stewart H.B.: *Nonlinear Dynamics and Chaos*. John Wiley
701 and Sons, New York, 376 pp., 1986.

702 Turcotte, D.L.: *Fractal and Chaos in Geology and Geophysics*, Cambridge Univ. Press,
703 New York, 221 pp., 1992.

704 Turcotte, D.L. and Schubert G.: *GEODYNAMICS – Applications of Continuum*
705 *Physics to Geological Problems*, Wiley, 450 pp., 1982

706 Wang, J.H.: Effect of seismic coupling on the scaling of seismicity, *Geophys. J. Int.*,
707 121, 475-488, 1995.

708 Wang, J.H.: Velocity-weakening friction law as a factor in controlling the
709 frequency-magnitude relation of earthquakes, *Bull. Seism. Soc. Am.*, 86,
710 701-713, 1996.

711 Wang, J.H.: Instability of a two-dimensional dynamical spring-slider model of an
712 earthquake fault, *Geophys. J. Int.*, 143, 389-394, 2000.

713 Wang, J.H.: A one-body model of the 1999 Chi-Chi, Taiwan, earthquake, *Terr. Atmos.*
714 *Ocean. Sci.*, 14(3), 335-342, 2003.

715 Wang, J.H.: Earthquakes rupturing the Chelungpu fault in Taiwan are time-
716 predictable, *Geophys. Res. Lett.*, 32, L06316 doi:10.1029/2004GL021884, 2005.

717 Wang, J.H.: A dynamic study of the frictional and viscous effects on earthquake
718 rupture: a case study of the 1999 Chi-Chi earthquake, Taiwan, *Bull. Seism. Soc.*
719 *Am.*,97(4), 1233-1244, 2007.

720 Wang, J.H.: One-dimensional dynamical modeling of earthquakes: A review, *Terr.*

721 Atmos. Ocean. Sci., 19, 183-203, 2008.

722 Wang, J.H.: Effect of thermal pressurization on the radiation efficiency, Bull. Seism.
723 Soc. Am., 99(4), 2293-2304, 2009.

724 Wang, J.H.: Thermal and pore fluid pressure history on the Chelungpu fault at a depth
725 of 1111 meters during the 1999 Chi-Chi, Taiwan, earthquake, J. Geophys. Res.,
726 116, B03302 doi:10.1029/2010JB007765, 2011.

727 Wang, J.H.: Some intrinsic properties of the two-dimensional dynamical spring-slider
728 model of earthquake faults, Bull. Seism. Soc. Am., 102(2), 822-835, 2012

729 Wang, J.H.: Slip of a one-body spring-slider model in the presence of slip-weakening
730 friction and viscosity, Ann. Geophys., 59(5), S0541, DOI:10.4401/ag-7063,
731 2016.

732 Wang, J.H.: Slip of a two-degree-of-freedom spring-slider model in the presence of
733 slip-weakening friction and viscosity, Ann. Geophys., 60(6), S0659, doi:10.
734 4401/ag-7295, 2017a.

735 Wang, J.H.: Frictional and viscous effects on the nucleation phase of an earthquake
736 nucleation, J. Seismol., 21(6), 1517-1539, 2017b.

737 Wang, J.H.: Multi-stable slip in a one-degree-of-freedom spring-slider model with
738 thermal-pressurized friction and viscosity, Nonl. Processes Geophys., 24,
739 467-480, doi.org/10.5194/npg-24-467-2017, 2017c

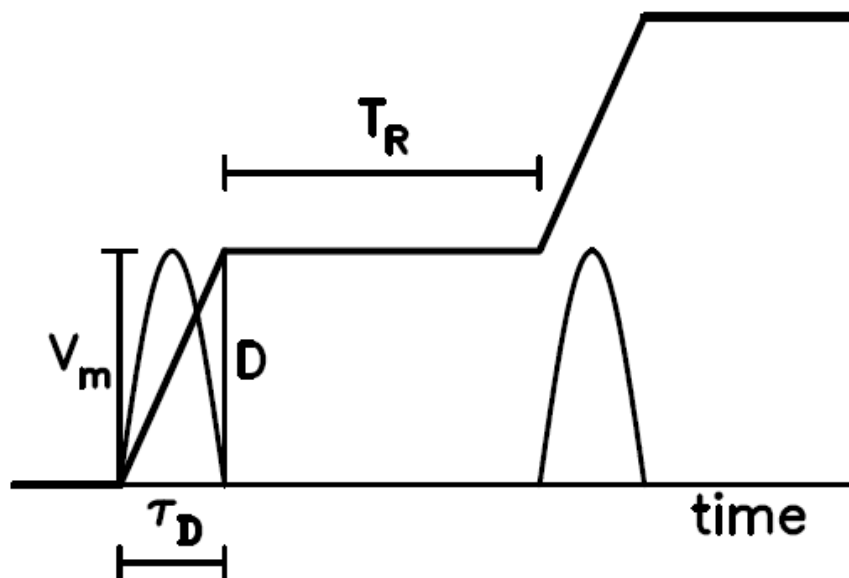
740 Wang, J.H. and Hwang R.D.: One-dimensional dynamical simulations of slip
741 complexity of earthquake faults, Earth Planets Space 53, 91-100, 2001.

742 Wang, J.H. and Kuo C.H.: On the frequency distribution of inter-occurrence times of
743 earthquakes, J. Seismol., 2, 351-358, 1998.

744 Ward, S.N.: A synthetic seismicity model for southern California: Cycles,
745 probabilities, and hazard, J. Geophys. Res., 101, 22393-22418, 1996.

746 Ward, S.N.: San Francisco Bay Area earthquake simulations: A step toward a
747 standard physical earthquake model, *Bull. Seism. Soc. Am.*, 90, 370-386, 2000.
748 Xu, H.J. and Knopoff L.: Periodicity and chaos in a one-dimensional dynamical
749 model of earthquakes, *Phys. Rev. E.*, 50(5), 3577-3581, 1994.
750

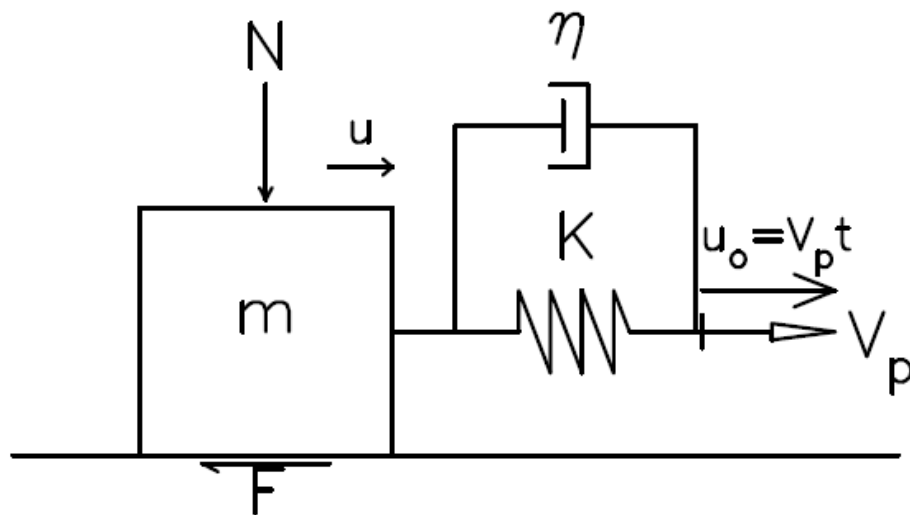
751
752
753



754
755
756
757
758
759
760

Figure 1. A general pattern of time variations in slip (thick solid line) and particle velocity (thin solid curve) during a seismic cycle: T_R =the recurrence time or the inter-event time of two events in a seismic cycle; τ_D =the duration time of slip of an event; D =the final slip of an event; and V_m =the peak particle velocity of an event.

761
762
763
764
765



766
767 Figure 2. One-body spring-slider model. In the figure, t , m , K , η , V_p , N , F , u , and u_o
768 denote, respectively, the time, the mass of the slider, the spring constant, the
769 damping coefficient, the driving velocity, the normal force, the frictional force,
770 displacement of the slider, and the equilibrium location of the slider. (after Wang,
771 2016)
772
773

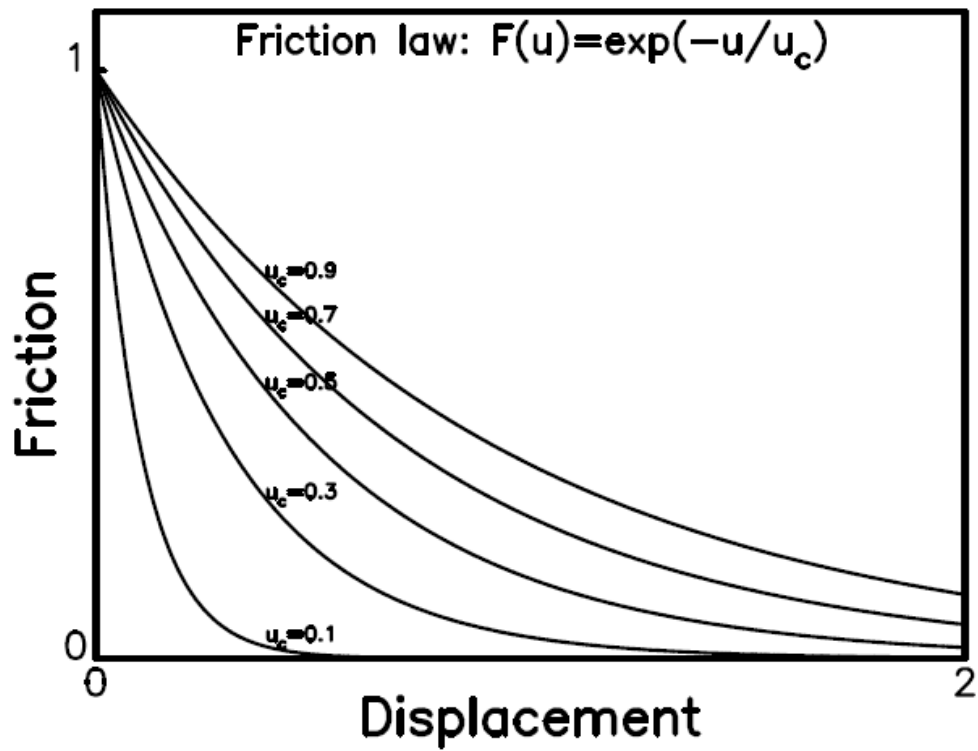
774

775

776

777

778



779

780 Figure 3. The plots of $F(u) = F_o \exp(-u/u_c)$ versus u when $u_c = 0.1, 0.3, 0.5, 0.7,$ and 0.9
781 m when $F_o = 1 \text{ Nt/m}^2$. (after Wang, 2016)

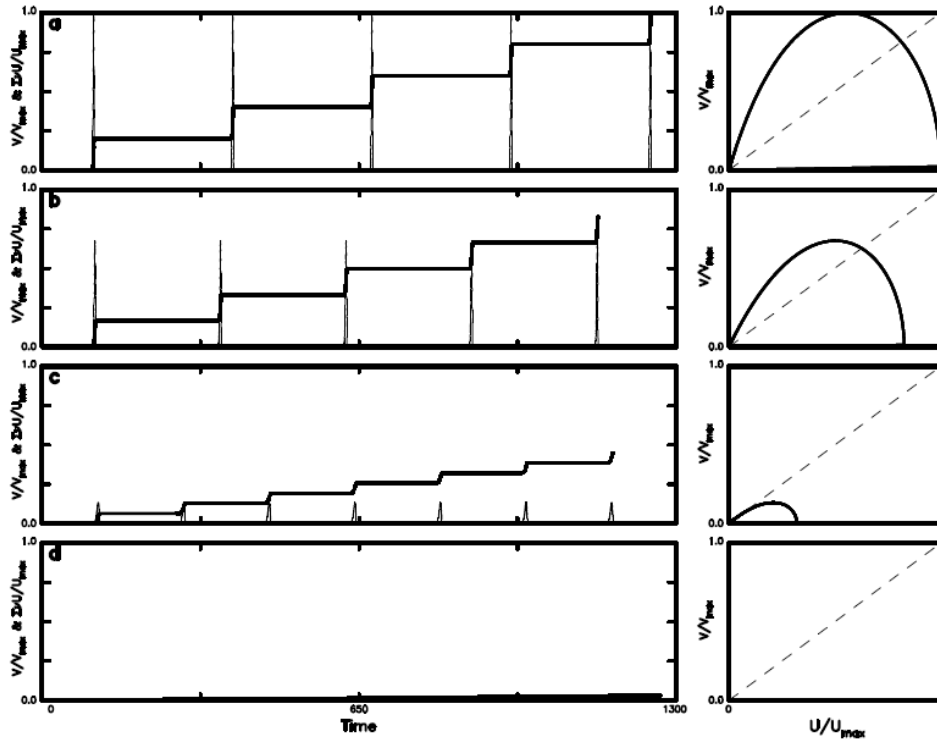
782

783

784

785

786



787

788 Figure 4. The time variations in V/V_{max} (thin solid line) and cumulative slip $\Sigma U/U_{max}$

789 (solid line) and the phase portrait of V/V_{max} versus U/U_{max} (solid line) for four

790 values of U_c : (a) for $U_c=0.2$; (b) for $U_c=0.4$; (c) for $U_c=0.8$; and (d) for $U_c=1.0$

791 when $\eta=0.0$.

792

793

794

795

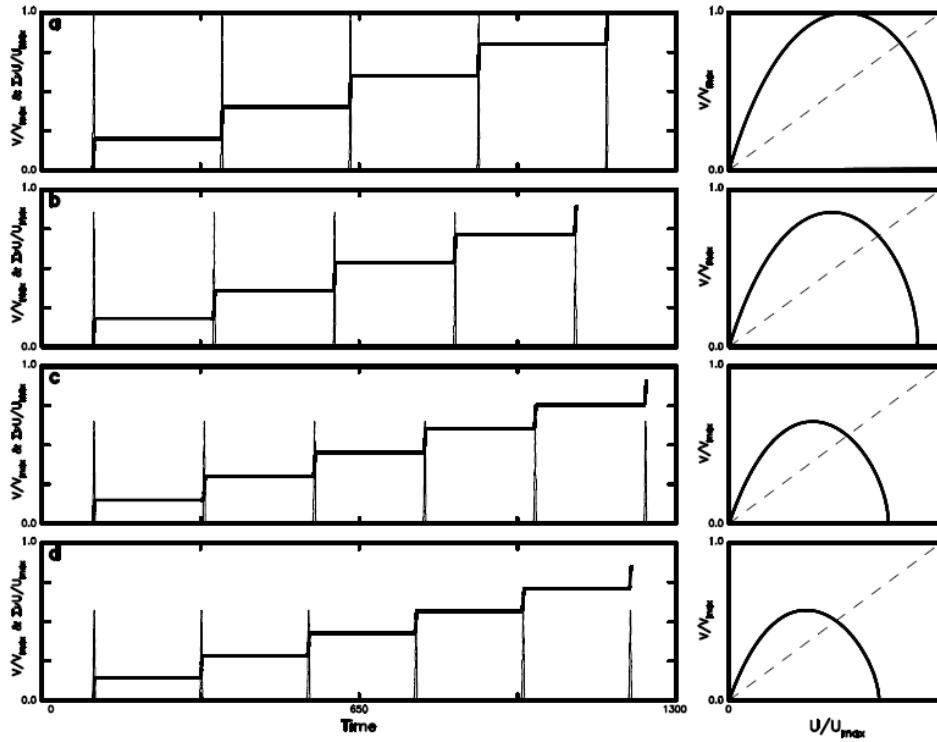
796

797

798

799

800



801

802 Figure 5. The time variations in V/V_{max} (thin solid line) and cumulative slip $\Sigma U/U_{max}$

803 (solid line) and the phase portrait of V/V_{max} versus U/U_{max} (solid line) for four

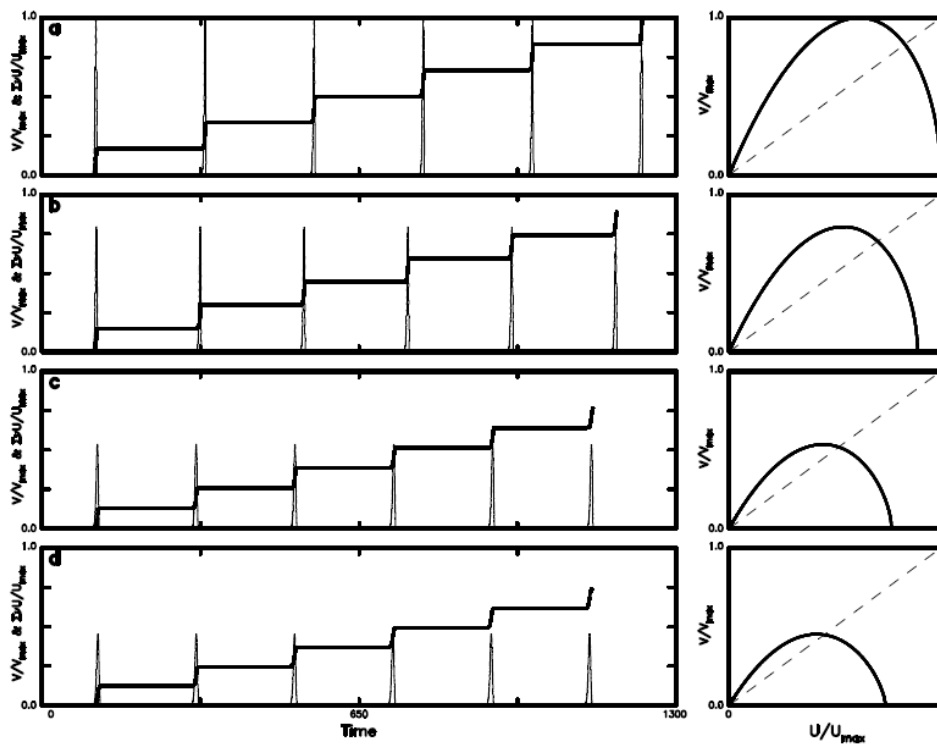
804 values of η : (a) for $\eta=0.2$; (b) for $\eta=0.4$; (c) for $\eta=0.8$; and (d) for $\eta=1.0$ when

805 $U_c=0.2$.

806

807

808
809
810



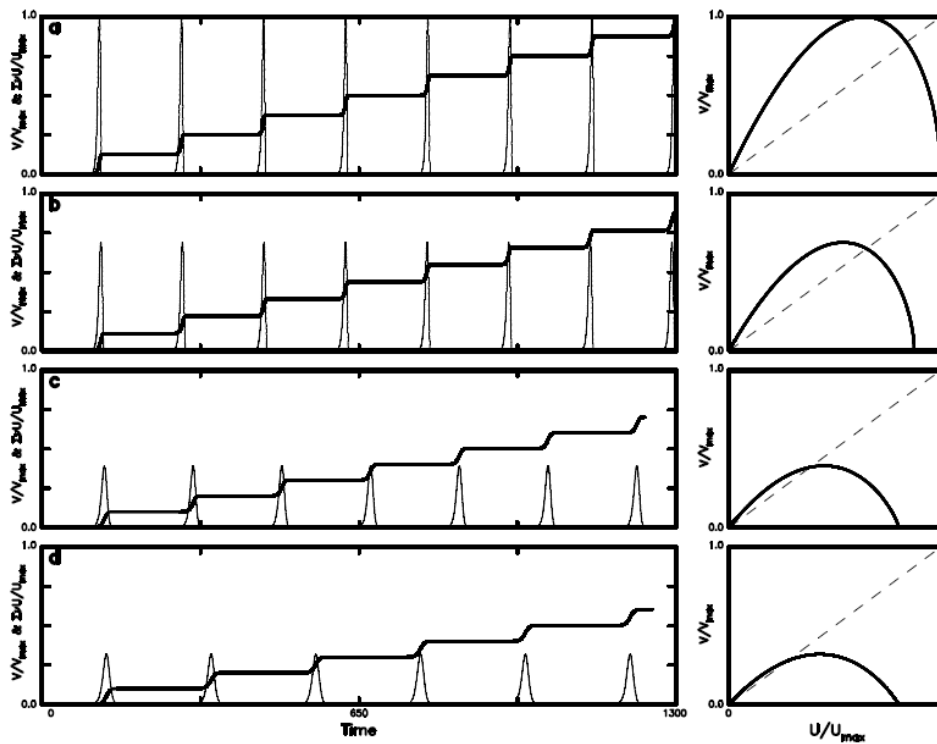
811
812
813
814
815
816

Figure 6. The time variations in V/V_{max} (thin solid line) and cumulative slip $\Sigma U/U_{max}$ (solid line) and the phase portrait of V/V_{max} versus U/U_{max} (solid line) for four values of η : (a) for $\eta=0.2$; (b) for $\eta=0.4$; (c) for $\eta=0.8$; and (d) for $\eta=1.0$ when $U_c=0.5$.

817

818

819



820

821 Figure 7. The time variations in V/V_{max} (thin solid line) and cumulative slip $\Sigma U/U_{max}$

822 (solid line) and the phase portrait of V/V_{max} versus U/U_{max} (solid line) for four

823 values of η : (a) for $\eta=0.2$; (b) for $\eta=0.4$; (c) for $\eta=0.8$; and (d) for $\eta=1.0$ when

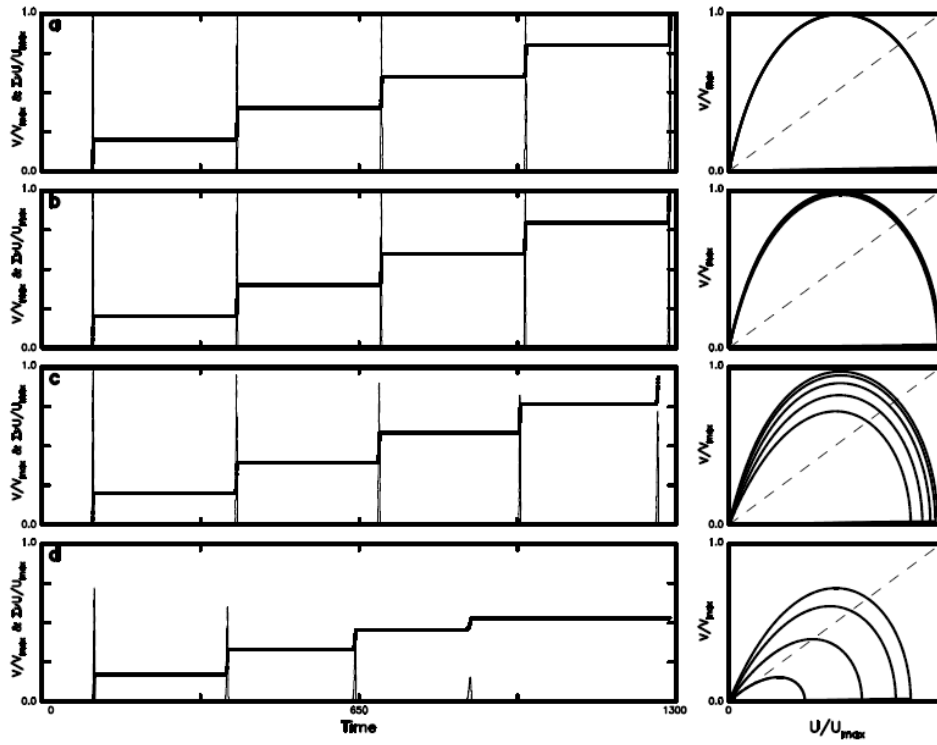
824 $U_c=0.8$.

825

826

827

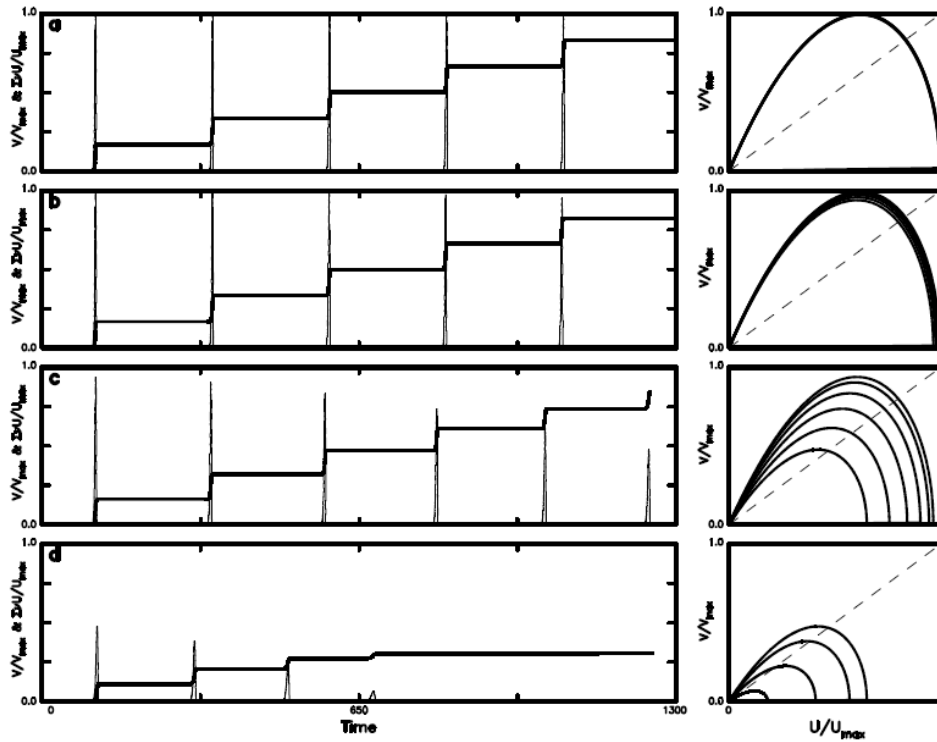
828
829
830



831
832
833
834
835
836

Figure 8. The time variations in V/V_{max} (thin solid line) and cumulative slip $\Sigma U/U_{max}$ (solid line) and the phase portrait of V/V_{max} versus U/U_{max} (solid line) for four values of C : (a) for $C=0.0001$; (b) for $C=0.001$; (c) for $C=0.01$; and (d) for $C=0.05$ when $U_{co}=0.1$ and $\eta=0$.

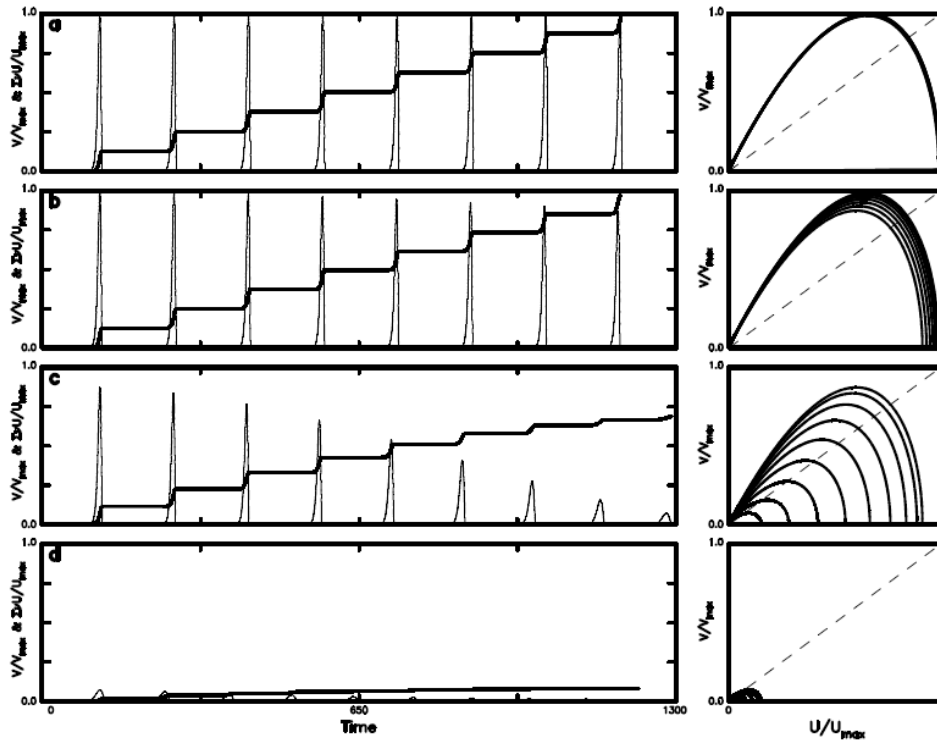
837
838
839



840
841
842
843
844
845

Figure 9. The time variations in V/V_{max} (thin solid line) and cumulative slip $\Sigma U/U_{max}$ (solid line) and the phase portrait of V/V_{max} versus U/U_{max} (solid line) for four values of C : (a) for $C=0.0001$; (b) for $C=0.001$; (c) for $C=0.01$; and (d) for $C=0.05$ when $U_{co}=0.5$ and $\eta=0$.

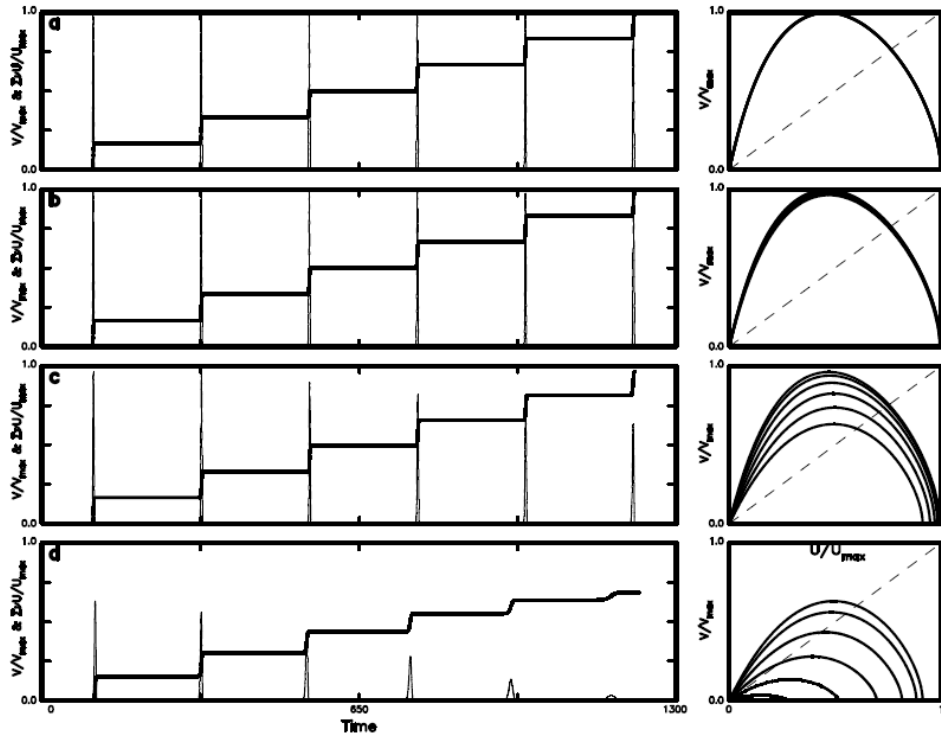
846
847
848



849
850
851
852
853
854

Figure 10. The time variations in V/V_{max} (thin solid line) and cumulative slip $\Sigma U/U_{max}$ (solid line) and the phase portrait of V/V_{max} versus U/U_{max} (solid line) for four values of C : (a) for $C=0.0001$; (b) for $C=0.001$; (c) for $C=0.01$; and (d) for $C=0.05$ when $U_{co}=0.9$ and $\eta=0$.

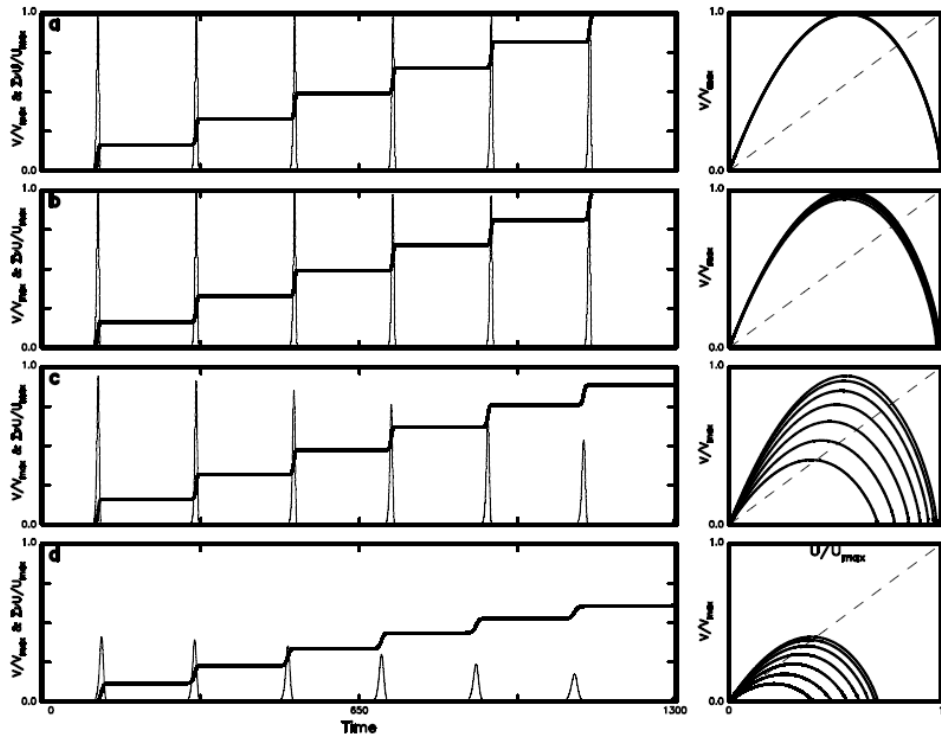
855
856
857



858
859
860
861
862
863

Figure 11. The time variations in V/V_{max} (thin solid line) and cumulative slip $\Sigma U/U_{max}$ (solid line) and the phase portrait of V/V_{max} versus U/U_{max} (solid line) for four values of C : (a) for $C=0.0001$; (b) for $C=0.0010$; (c) for $C=0.0100$; and (d) for $C=0.0380$ when $U_{co}=0.1$ and $\eta=1$.

864
 865
 866
 867



868
 869
 870
 871
 872
 873
 874

Figure 12. The time variations in V/V_{max} (thin solid line) and cumulative slip $\Sigma U/U_{max}$ (solid line) and the phase portrait of V/V_{max} versus U/U_{max} (solid line) for four values of C : (a) for $C=0.0001$; (b) for $C=0.0010$; (c) for $C=0.0100$; and (d) for $C=0.0136$ when $U_{co}=0.5$ and $\eta=1$.